JOURNAL OF SYNCHROTRON RADIATION
ISSN 1600-5775

First results from the XMCD facility at the Energy-Dispersive EXAFS beamline of the Indus-2 synchrotron source

N. Patra,[a,b] U. G. P. S. Sachan,[c] S. SundarRajan,[c] Sanjay Malhotra,[c] Vijay Harad,[c] Ankur Agarwal,[a] Ashutosh Divedi,[a] S. N. Jha[a] and D. Bhattacharyya[a]*

[a]Atomic and Molecular Physics Division, Bhabha Atomic Research Centre, Mumbai 400 085, India, [b]Homi Bhabha National Institute, Anushaktinagar, Mumbai 400 094, India, and [c]Accelerator Control Division, Bhabha Atomic Research Centre, Mumbai 400 085, India. *Correspondence e-mail: dibyendubarc@gmail.com

Received 5 September 2018
Accepted 11 January 2019

Edited by R. W. Strange, University of Essex, UK

Keywords: XMCD; EXAFS beamline; Indus-2; synchrotron radiation.

Setting up of the X-ray Magnetic Circular Dichroism (XMCD) measurement facility with hard X-rays at the Energy-Dispersive EXAFS beamline (BL-08) at the Indus-2 synchrotron source is reported. This includes the design and development of a water-cooled electromagnet having a highest magnetic field of 2 T in a good field volume of 125 mm^3 and having a 10 mm hole throughout for passage of the synchrotron beam. This also includes the development of an (X–Z–θ) motion stage for the heavy electromagnet for aligning its axis and the beam hole along the synchrotron beam direction. Along with the above developments, also reported is the first XMCD signal measured on a thick Gd film in the above set-up which shows good agreement with the reported results. This is the first facility to carry out XMCD measurement with hard X-rays in India.

1. Introduction

X-ray magnetic circular dichroism (XMCD) is a powerful spectroscopic technique which is widely used for studying both the localized and itinerant magnetism of a magnetic material and is rapidly becoming popular for probing the magnetic properties of materials as diverse as molecular magnets, multilayers, nanoparticles, *etc*. (Jo & Sawatzky, 1991; Guo, 1996; van der Laan & Figueroa, 2014). Unlike other dichroism techniques such as the Kerr effect or the Faraday effect where visible light is used as a probe, XMCD uses X-rays as a probe taking advantage of the orbital and element selectivity properties of X-ray absorption spectroscopy (Stöhr, 1999). The absorption process in the XMCD measurement is a two-step model where in the first step the polarized X-ray photon (left circularly polarized or right circularly polarized) transfers angular momentum ($+h$ or $-h$) to the spin–orbit-coupled core-level electrons. Next these two different spin polarized photoelectrons are excited to the valance band according to the selection rules. Thus, the difference in the absorption spectra between the two orthogonal polarizations reflects the valence band spin-up and spin-down density of states. The measurements can be carried out by flipping the direction of the magnetic field and using the same polarization state of the X-rays or by keeping the magnetic field constant and changing the polarization state of the X-ray beam. In a ferromagnetic material the density of states at the Fermi level is spin dependent and so a difference in the absorption for the left and right circularly polarized light for a ferromagnetic material is expected. Also, as XMCD is associated with the X-ray

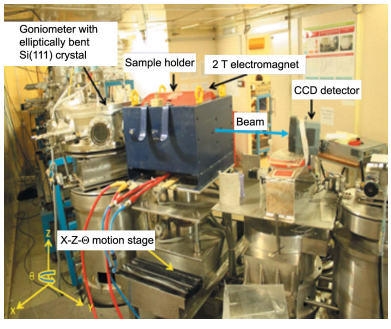

absorption technique, it not only probes the magnetic structure of the atom but also simultaneously provides the electronic properties and the local structural information around the constituent atoms. Synchrotron radiation from a bending-magnet source is usually linearly polarized in the plane of the electron orbit. Opposite helicities of circular polarization occur just above and below the orbit plane. These well defined polarization states make synchrotron radiation a powerful technique in polarization-dependent scattering or absorption, such as XMCD.

In the Dispersive EXAFS beamline (BL-08) at the Indus-2 synchrotron radiation source (SRS), measurements at the *K*-edge of the transition metals (3*d*) and the $L_{2,3}$-edges of the rare-earth elements (5*d*) are possible (Bhattacharyya *et al.*, 2009). One major advantage of the Dispersive EXAFS beamline is that there are no moving parts during the data acquisition and hence the data are not affected by any artifact arising from motor movements. However, in the Dispersive EXAFS beamline the measurements can only be made in transmission mode, which imposes some restrictions on the thickness and uniformity of the samples. However, the data obtained from measurement in transmission mode are free from self-absorption effects or any defects or perturbation on the surface which are common in the case of fluorescence yield (FY) or total electron yield (TEY) measurement modes. Another advantage of the Dispersive EXAFS beamline (BL-08) is that, due to the horizontal dispersion geometry of the beamline, it uses a vertically tall beam at the entrance of the beamline which helps to select the highest and the lowest portion of the beam with well defined polarizations using a precision slit. XMCD measurements in transmission geometry in energy-dispersive-type beamlines have been reported previously (Baudelet *et al.*, 2016; Cezar *et al.*, 2010). Additionally, as has been mentioned above, XMCD measurement needs a sufficiently strong external magnetic field to saturate the magnetic states of the material under investigation.

Here we present details of setting up the XMCD measurement facility at the Energy-Dispersive EXAFS beamline (BL-08) at the Indus-2 synchrotron radiation source and the first signal observed from the measurement. The setup has been tested by carrying out XMCD measurements on a thick Gd film, since several reports are available in the literature for room-temperature XMCD measurements at the L_2- or L_3-edge of Gd for comparison (Koizumi *et al.*, 2000; Boada *et al.*, 2010; Haskel *et al.*, 2007; Tolentino *et al.*, 1998).

2. Development of the electromagnet

To carry out the XMCD measurements a dipole magnet of maximum field 2 T in a good field volume (GFV) of 125 mm^3 has been developed. The overall size of the magnet is 500 mm × 500 mm × 400 mm and its weight is about 400 kg. Considering the field requirement, structural geometry, uniformity of the magnetic field within a certain volume and cooling process, the design of the magnet has been carried out. Pole shape optimization has been carried out to achieve a field uniformity of 100 p.p.m. in the required GFV. Along with this a motorized *X*–*Z*–θ motion stage has been used for alignment and rotation of the electromagnet axis with the beam direction to facilitate studies at different magnetization angles of the sample. The overall system has been designed in such a way that the field remains constant for the duration of the X-ray absorption scan running with a constant current. The whole magnetic system consists of several components, such as magnet coil, magnet core, cooling system and support system.

2.1. Electromagnet design

The basic requirements for the design of the electromagnet have been listed in Table 1. A detailed electromagnetic design for optimization of the magnet yoke and poles (taper and diameter) for the required magnetic peak field in the magnet center was carried out using the software package *TOSCA* (Electromagnetic Analysis Software, Vector Fields Inc., Oxford, UK). Figs. 1(*a*) and 1(*b*) show the model for the EM analysis and the variation of the magnetic field uniformity at the air gap between the poles. A 10 mm central bore was made in the magnet poles for the X-ray beam to pass through. Generally in this configuration the incident beam direction is parallel to the direction of the applied magnetic field. The magnetic core is made out of low-carbon steel plates, while the pole pieces were made of soft pure iron rods. EM simulations were carried out to optimize magnet dimensions and the pole taper angle for meeting the objective of good field uniformity in the GFV. A pole taper angle of 37° was found to be the most optimum for field uniformity and matches with the theoretical estimates (Arenholz & Prestemon, 2005; Fiorillo, 2004). The minimum field increment of the electromagnet is limited by the step size of the power supply current. Thus, the magnet was designed for field uniformity over the sampled area of the X-ray beam in the geometry.

2.2. Coil design

The input ampere turns required for the development of a 2 T magnet is 48000 A T. Hence a standard oxygen-free electronic (OFE) grade Cu conductor with a 12 mm × 12 mm square cross section with 6 mm central hole was selected. The thickness of the wire was determined by its mechanical strength. All the electrical terminals were located at the base of the coil for the power supply. These hollow Cu conductors were arranged in a Helmholtz configuration. The joule dissipation by the Cu wire at nominal current is 5 kW, which is removed by demineralized water (flow speed of 2 m s^{-1} at a pressure of 3 bar). The maximum reachable field is limited by the ability to remove the power dissipation in the magnetic coil by water cooling.

Thus, based on the above design, development of the electromagnet was carried out. The cross-sectional details of the magnet and magnetic field uniformity are shown in Fig. 2. To carry out the winding of the solenoid coils, suitable jigs were developed. The interlayer insulation was made of glass fiber tapes and the coil was epoxy impregnated to provide better mechanical strength.

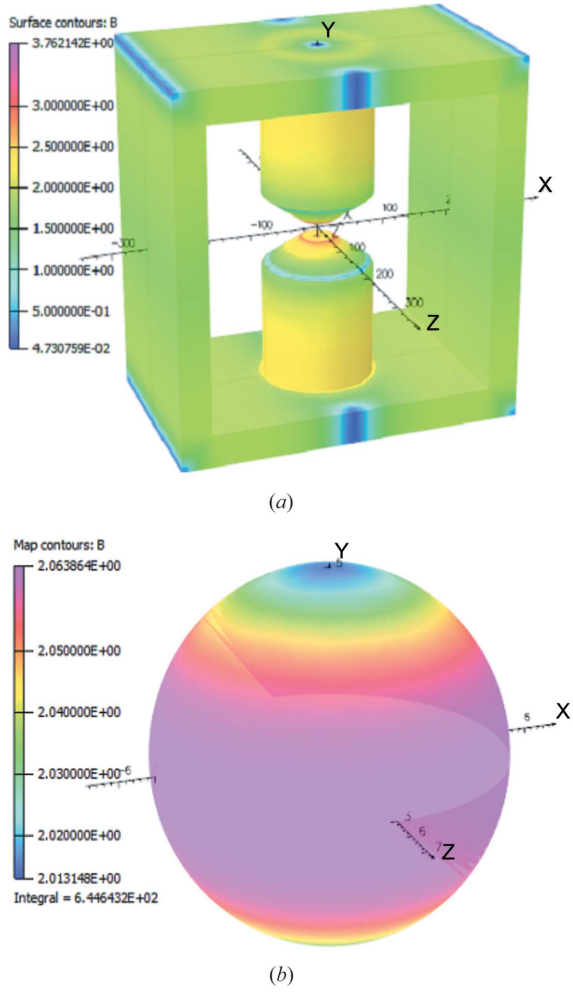

Figure 1
(*a*) Magnetic field in the core at nominal current. (*b*) Magnetic field uniformity in the good field volume (better than 100 p.p.m.).

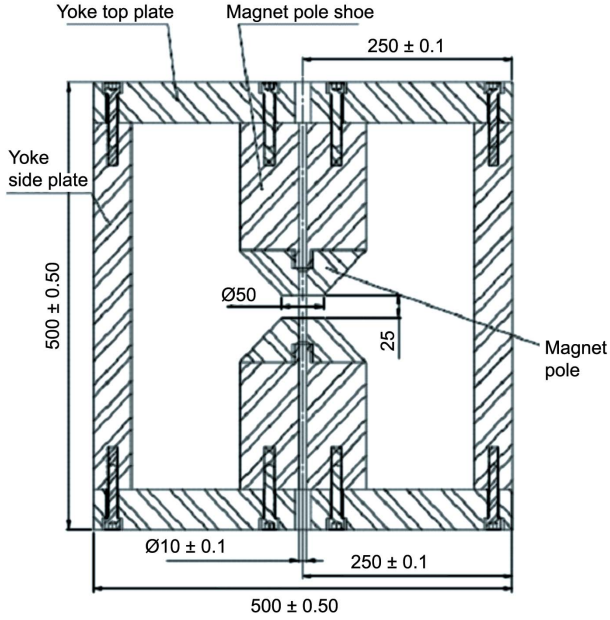

Figure 2
Details of the electromagnet cross section (dimensions are in mm).

Table 1
Specifications of the electromagnet.

Central magnetic field	2 T
Air gap	25 mm
Good field volume	125 mm^3
Magnetic field uniformity	$<$100 p.p.m.
Magnet shape	H-dipole
Magnet outer dimensions	500 mm $\times$ 500 mm $\times$ 400 mm

2.3. Development of magnet mounting motion stage

A motorized motion stage has been developed for easy and perfect alignment of the axis as well as the beam hole of the heavy electromagnet with that of the synchrotron beam, and also to facilitate studies on different magnetization angles of the sample. The stage can provide X–Z and θ rotation. Here the X motion is the horizontal movement perpendicular to the direction of the beam, Z is the vertical movement and θ is the angle between the beam and the magnet axis about a vertical axis. The movement along the X direction across the beam is achieved through an arrangement with ball screw and nut with linear guides, which has a stroke of $\pm$50 mm and a resolution of 10 µm, while the motion along the Z direction is made possible by a worm gear box along with ball screw and nut with a shaft stroke of $\pm$15 mm and resolution of 10 µm. The θ rotation has a stroke of $\pm20^\circ$ and a resolution of 0.01°, accomplished by a worm gear box. All the motions are remotely computer controlled and measured by independent encoders. Fig. 3 shows a photograph of the motion stage.

2.4. Testing of the electromagnet

The electromagnet was tested for its operating performance by increasing the current through the coil up to 300 A. The polarity of the electromagnet was changed by quickly switching at the same current, so that the intensity of the incident X-ray beam does not change within the operation. The flow rate and temperature difference between the inlet and outlet were measured, and were found to agree closely

Figure 3
The X–Z–θ motion stage, which can carry a maximum of 500 kg.

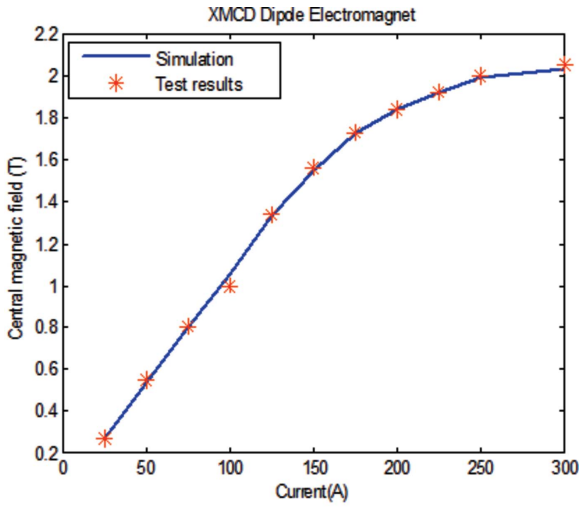

Figure 4
Simulated and measured magnetic field in the air gap.

with the design estimates. The central magnetic field was measured with a Hall sensor. A good agreement between the measured and simulated magnetic field at the air gap is shown in Fig. 4.

3. Experimental description of the Energy-Dispersive EXAFS beamline at Indus-2

The Energy-Dispersive EXAFS beamline operates within the photon energy range 5–20 keV which provides energy bandwidths of 0.3, 1.0 and 2.0 keV at photon energies 5, 10 and 20 keV with resolution of 0.5, 1.0 and 2 eV. The beamline consists of a 460 mm-long Si(111) ($2d$ = 6.2709 Å) crystal mounted on an elliptical crystal bender (B_1, B_2) and a position-sensitive CCD detector of size 25 mm × 25 mm having 2048 × 2048 pixels. The Si crystal was chosen because of its narrow Darwin width, low thermal expansion coefficient and high thermal conductivity as a polychromator. The optical layout of the beamline is shown in Fig. 5.

In the beamline the Si(111) crystal C is bent in such a way that the source of the beam S_0 and the sample position S_2 remain at the two foci of the ellipse. This ensures that all the radiation emerging from the source S_0 reaches S_2 with minimum aberration. A beam aperture (A) made of water-cooled copper blocks and a precision slit system (S_1) which uses two sets of water-cooled tantalum jaws define the final horizontal and vertical divergences of the beam coming from the bending magnet through the Be window (B). After emerging from the slit system the beam having certain horizontal and vertical divergence falls on the Rh-coated cylindrical mirror M_1 at a grazing angle of incidence of ∼0.2°. This mirror is used for the vertical focusing of the beam at the sample position and to cut off the higher-energy part of the beam. After being reflected from the mirror the horizontally diverging beam falls on the Si crystal (C) and, depending upon the radius of curvature of the crystal and the angle of incidence, the crystal reflects a particular band of energy (ΔE). Finally, this spatially dispersed polychromatic radiation is

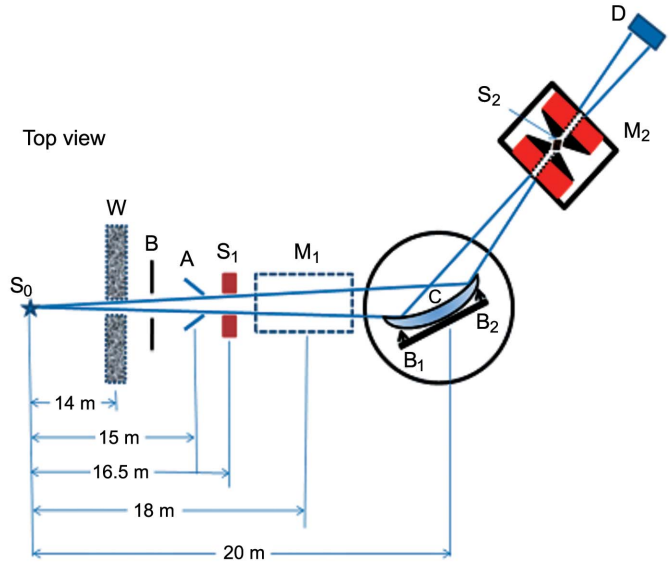

Figure 5
Top view of the beamline with electromagnet.

focused at the sample position (S_2) due to the elliptical curvature of the crystal. After transmission through the sample the beam diverges further and falls on the position-sensitive detector (D). The whole setup of the beamline after the mirror is mounted on a goniometer; while the crystal chamber is mounted on its θ axis, the sample stage and the detector stages are mounted on the 2θ arm. Thus the energy-dispersive X-ray absorption spectra are recorded by the detector over a wide energy range (ΔE) around a central energy (E_0). Detailed calculations of the beamline parameters have been given elsewhere (Bhattacharyya *et al.*, 2009).

For the present measurement, the electromagnet has been placed in the beamline in such a way that the sample position, *i.e.* the focal point of the bent crystal (S_2), coincides with the zone of uniform magnetic field as shown in Fig. 5. In this case the electromagnet, being very heavy (approximate weight: 400 kg), has not been placed on the 2θ arm of the goniometer. Instead it is placed on a specially designed X–Z–θ motion stage, described above, while the detector is placed on the 2θ arm. The motions of the motion stage of the electromagnet are synchronized with the movement of the detector position. The motorized stage of the electromagnet not only helps to align the axis of the magnetic field parallel to the beam but also facilitates studies on different magnetization angles of the sample. As has been mentioned earlier, for the present measurement we have selected the top portion of the beam using the slit system prior to the mirror to select right-circularly polarized beam for the XMCD measurement under forward and reverse magnetic fields. A photograph of the whole setup is shown in Fig. 6. The setup has been tested by measuring the XMCD signal of a thick Gd film.

4. Results and discussion

For transmission mode measurement the absorption coefficient (μ) is obtained as $\mu = \ln(I_0/I_t)$ where I_0 and I_t are the

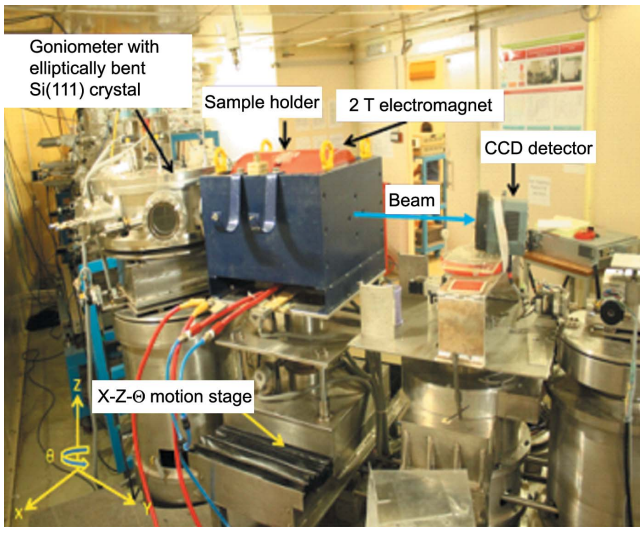

Figure 6
Photograph of the Energy-Dispersive EXAFS beamline with the magnet installed at the sample position.

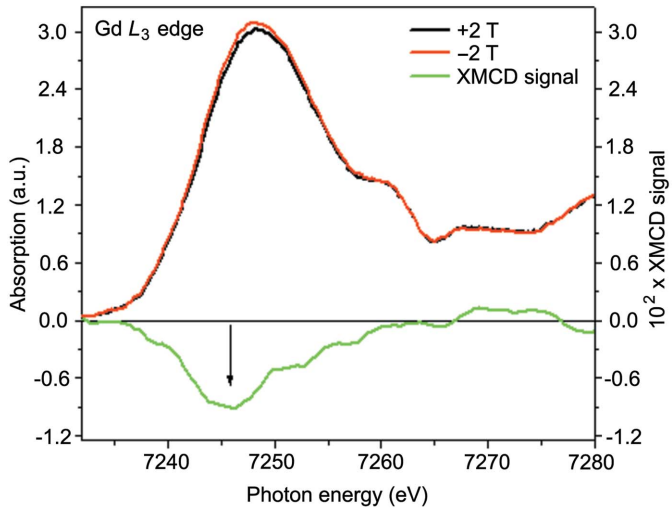

Figure 7
Normalized XANES spectra and the magnified XMCD signal of a thick Gd film.

intensities of the photon beam at a particular CCD pixel without and with the sample. The XMCD signal is obtained as $\mu^+ - \mu^-$ for two different polarities of the electromagnet (positive and negative) at a certain polarization of the incident X-rays. To reduce the symmetric error the scan at constant magnetic field was taken 50 times and averaged. The CCD channel numbers have been calibrated to the energy scale by measuring the absorption edges of a standard Fe foil and Gd L_3-edge of standard Gd_2O_3 powders having nominal K and L_3 energy edges at 7112 eV and 7243 eV, respectively. Finally, the setup has been tested by measuring the XMCD signal of a ~4 µm-thick Gd film prepared by DC magnetron sputtering of a 99.99% pure Gd metallic target on an Al foil substrate. The foil was mounted on a rigid Teflon support with a hole at the center for passage of the synchrotron beam and was placed at the center of the air gap between two magnetic poles by holding the Teflon support by a custom-made Teflon holder.

Fig. 7 shows the normalized XANES spectra and the XMCD signal of the Gd foil taken at a magnetic field of 2 T by switching the polarity of the electromagnet. The magnitude of the field was chosen so that the magnetic moments saturate. It has been observed that the XMCD signal profile of the thick Gd film agrees well with that reported by other workers (Koizumi *et al.*, 2000).

5. Conclusions

An X-ray magnetic circular dichroism measurement facility with hard X-rays has been set up at the Energy-Dispersive EXAFS beamline (BL-08) at the Indus-2 synchrotron source. A water-cooled electromagnet having a highest magnetic field of 2 T in a good field volume (GFV) of 125 mm^3 and having a 10 mm hole throughout for passage of the synchrotron beam has been developed. The heavy electromagnet is aligned with the synchrotron beam using a custom built (X–Z–θ) motion stage having computer-controlled precision movement facilities. The setup has been successfully tested by measuring the XMCD signal of a Gd thick film which shows good agreement with reported results.

Acknowledgements

The authors wish to acknowledge the contributions of Dr A. Biswas and Mrs P. Sarkar of A&MPD, BARC, for their help in depositing the Gd thick film.

References

Arenholz, E. & Prestemon, S. O. (2005). *Rev. Sci. Instrum.* **76**, 083908.
Baudelet, F., Nataf, L. & Torchio, R. (2016). *High. Press. Res.* **36**, 429–444.
Bhattacharyya, D., Poswal, A. K., Jha, S. N., Sangeeta & Sabharwal, S. C. (2009). *Nucl. Instrum. Methods Phys. Res. A*, **609**, 286–293.
Boada, R., Laguna-Marco, M. Á., Gallastegui, J. A., Castro, G. R. & Chaboy, J. (2010). *J. Synchrotron Rad.* **17**, 308–313.
Cezar, J. C., Souza-Neto, N. M., Piamonteze, C., Tamura, E., Garcia, F., Carvalho, E. J., Neueschwander, R. T., Ramos, A. Y., Tolentino, H. C. N., Caneiro, A., Massa, N. E., Martinez-Lope, M. J., Alonso, J. A. & Itié, J.-P. (2010). *J. Synchrotron Rad.* **17**, 93–102.
Fiorillo, F. (2004). *Measurement and Characterization of Magnetic Materials*, ch. 4. San Diego: Elsevier.
Guo, G. Y. (1996). *J. Phys. Condens. Matter*, **8**, L747–L752.
Haskel, D., Tseng, Y. C., Lang, J. C. & Sinogeikin, S. (2007). *Rev. Sci. Instrum.* **78**, 083904.
Jo, T. & Sawatzky, G. A. (1991). *Phys. Rev. B*, **43**, 8771–8774.
Koizumi, A., Takagaki, M., Suzuki, M., Kawamura, N. & Sakai, N. (2000). *Phy. Rev. B*, **61**, R14909.
Laan, G. van der & Figueroa, A. I. (2014). *Coord. Chem. Rev.* **277–278**, 95–129.
Stöhr, J. (1999). *J. Magn. Magn. Mater.* **200**, 470–497.
Tolentino, H., Cezar, J. C., Cruz, D. Z., Compagnon-Cailhol, V., Tamura, E. & Martins Alves, M. C. (1998). *J. Synchrotron Rad.* **5**, 521–523.